The *ac*-Josephson relation and inhomogeneous temperature distributions in large $Bi_2Sr_2CaCu_2O_{8+\delta}$ mesas for THz-emission

T. M. Benseman, A. E. Koshelev, W.-K. Kwok, U. Welp

Materials Science Division, Argonne National Laboratory, Argonne IL 60439

K. Kadowaki

Institute for Materials Science, University of Tsukuba, Ibaraki 305-8753, Japan

J. R. Cooper

Cavendish Laboratory, University of Cambridge, Cambridge CB3 0HE, UK

G. Balakrishnan

Department of Physics, University of Warwick, Coventry CV4 7AL, UK

We have studied the terahertz emission from a $720 \times 60 \times 1.2$ μm^3 mesa patterned from underdoped $Bi_2Sr_2CaCu_2O_{8+\delta}$. This device has an S-shaped current-voltage characteristic due to self-heating, allowing us to compare its THz emission behavior at up to three different bias currents for the same voltage. The THz frequency generated along the lowest current branch follows the expected Josephson relation for a stack of intrinsic Josephson junctions connected in series. However, in the high current regimes, THz is emitted at a significantly lower frequency than expected. We show that this behavior is consistent with strongly non-uniform self-heating of the mesa at high bias currents.

The observation [1] of the emission of coherent, continuous-wave THz-radiation from stacks of intrinsic Josephson junctions (IJJs) [2] in the layered high-T_c superconductor $Bi_2Sr_2CaCu_2O_{8+\delta}$ (Bi-2212) has generated considerable interest in the collective dynamics of large IJJ arrays [3-14]. The relatively large values of the off-chip radiation powers of tens of microwatts [11, 14] indicate that a substantial fraction of the IJJs in the stack are synchronized and emit coherently. The observed emission frequencies range from ~0.4 THz to ~1 THz and are found to scale inversely with the width of the junction stacks [1, 8, 11] suggesting that an electromagnetic cavity resonance promotes the synchronization of the junctions [15]. Junction stacks for THz-emission have typical sizes of ~1 – 2 μm height, corresponding to roughly 1000 IJJs, and lateral dimensions ~50 to 100 μm in width and several 100 μm in length. Extensive work [16] has established that such stacks of IJJs are prone to strong self-heating effects most clearly evidenced by the pronounced S-shape of their current-voltage characteristics. Two regimes of THz-emission from IJJ-stacks have been identified: the low-bias regime where self-heating effects can be neglected and the temperature in the stack is essentially uniform and close to the cryostat temperature, and the high-bias regime where self-heating causes strongly non-uniform temperature distributions inside the stack. Low temperature scanning laser microscopy (LTSLM) [4, 6, 8], thermal imaging [14, 17] as well as solutions to the heat diffusion equation [18, 19] reveal hot spots in which the temperature can exceed T_c and that are accompanied by large lateral temperature gradients. Nonetheless, it has been shown that in the low as well as in the high bias regimes the *ac*-Josephson relation in terms of the voltage applied across the stack is

fulfilled [9, 11, 13]. This implies that the voltage per junction and the temperature distribution are uniform along the thickness of the stack.

Here we present results on *c*-axis transport and THz-emission on a 60 x 720 μm^2 mesa patterned onto a slightly under-doped Bi-2212 crystal. Polycrystalline phase-pure Bi-2212 powder was prepared in Cambridge. At the University of Warwick the powder was pressed into feed rods 5 mm in diameter, and single crystals were grown by the traveling solvent floating zone method. (Details of powder preparation, crystal growth, and the properties of the resulting crystals are given in [20] and [21].) At Argonne mesa devices were patterned on the surface of the crystal using photolithography and Ar-ion milling. The height of the mesa is ~1.2 μm. The emission frequency in the high-bias regime shows unexpected re-entrant behavior and deviation from the *ac*-Josephson relation in terms of applied voltage indicating that temperature gradients in the vertical direction are important. Our results can be explained in a model in which the stack is composed of colder layers near its bottom and hot layers near its top. This model also accounts for the observation that emission persists up to bias currents at which the average stack temperature exceeds T_c by a factor of two.

Fig. 1 shows the temperature dependence of the *c*-axis resistance of the IJJ stack measured with a current of 10 μA. The monotonic increase of the resistance with decreasing temperature, as well as the value of $T_c \sim 65$ K are indicative of the under-doped nature of the material. Below the superconducting transition the resistance again increases with further decreasing temperature, which we attribute to non-superconducting junctions at the top of the mesa. The inset of Fig. 1 shows the

return branches of the current-voltage characteristics measured at various temperatures between 10 K and 100 K. Here, the voltage values have been corrected for a contact resistance of 3.3 Ω, corresponding to the value of R_c just below T_c; see the Appendix for a detailed discussion of the contact resistance. The pronounced back-bending of the IV-curves is a manifestation of significant self-heating as has been described extensively before for large mesas [16, 18, 19]. At temperatures below 45 K we can distinguish three regimes: the 'normal' regime at the bottom of the IV-curves, the back-bending regime at intermediate bias currents characterized by $\partial I/\partial V < 0$, and the forward-bending regime at very high current bias with $\partial I/\partial V > 0$. A feature typically not seen in IV-curves of such large mesas is the fact that re-trapping occurs at relatively low voltages such that the return branch approaches a linear curve through the origin (solid line in Fig. 1) enabling the estimation of the *c*-axis resistance at temperatures below T_c from the sub-gap resistance. The results, included in the main panel of Fig. 1 as orange squares, reveal that at low temperatures the *c*-axis resistance saturates and increases approximately linearly with decreasing temperature [22] at a rate of ~ 3.8 Ω/K.

Owing to the S-shape of the IV-curves there are – in principle – up to three working points for a given mesa voltage at which THz-emission can occur [23]. This is indeed the case as shown in the FTIR spectra (Fig. 2) taken at 15 K and bias voltages of 1.018 V and 1.037 V. Three sets of emission lines at different frequencies and corresponding to the 'normal', back-bending and forward-bending regimes, respectively, are clearly resolved. The emission lines near 19 cm^{-1} are in good agreement with previous results on 60-μm wide mesas [1].

The evolution of the emission frequency with bias voltage and temperature is summarized in Fig. 3a. The corrections for the contact resistance are described in detail in the appendix. The linear dependence in the 'normal' regime (top left) is expected on the basis of the *ac*-Josephson relation [9, 11, 13], which – in the units of Fig. 3a – reads $1/\lambda = 16120\,(Vcm)^{-1}\,V_{jct}$. In the 'normal' regime self-heating can be neglected, and the mesa can be considered as a uniform system. Then the junction voltage V_{jct} is related to the mesa voltage V through $V_{jct} = V/N$, where N is the number of junctions in the mesa. Thus, the slope of the $1/\lambda$-data of ~17.5 $(Vcm)^{-1}$ implies a junction number of N~920, in good agreement with the physical size of the sample. The frequency data at 10 K follow a linear dependence with slightly higher slope corresponding to about 2 % fewer emitting junctions.

In the back-bending and forward-bending regions the emission frequency does not follow the Josephson relation as function of mesa voltage. This is a manifestation of the fact that the mesa voltage is no longer related in a simple way to the junction voltage, since the system has become inhomogeneous. LTSM [5, 7, 9], thermal imaging [14, 17] as well as numerical solutions of the heat diffusion equation [18, 19] indicate a strongly non-uniform lateral temperature distribution under bias conditions corresponding to the back-bending and forward-bending regimes. The strong temperature dependence of the *c*-axis resistivity can cause an electro-thermal instability accompanied by the formation of hot-spots that are characterized by a strongly enhanced temperature and current density as compared to the rest of the mesa. Nevertheless, due to the very large anisotropy of the in-plane and out-of-plane resistivities of BSCCO we can consider the *ab*-planes as

equipotentials. Thus, even in the presence of large in-plane temperature gradients the voltage per junction would be uniform along the *c*-axis, and the Josephson relation in terms of the mesa voltage would apply. This has been observed in previous reports [9, 11, 13]. In contrast, the data in Fig. 3a indicate non-uniformity along the *c*-axis.

The mere fact that we observe THz-emission at reasonably high power in the back-bending region implies that a large fraction of the junctions in the mesa are synchronized. The voltage per junction in this group of synchronized junctions is reduced with respect to emission in the 'normal' region by the ratio of emission frequency for the same mesa voltage. For example, at 1.037 V across the mesa the emission frequency, and therefore the junction voltage of the emitting junctions, is reduced by a factor of k_1 = 0.93. Generally, one finds that in the 'normal' region the voltage across the stack is given as $V_0 = NV_{jct,0} = NI_0 r_{jct,0}$ whereas in the back-bending regime it is $V_1 = N_1 V_{jct,1} + (N - N_1) I_1 \bar{r} = N_1 I_1 r_{jct,1} + (N - N_1) I_1 \bar{r}$ (see Fig. 3b). Here, $V_{jct,0}$ and $V_{jct,1}$ are the junction voltages at bias currents I_0 and I_1 in the 'normal' region and of the N_1 emitting junctions in the back-bending region, respectively, and $\bar{r}$ is the average junction resistance of the $(N\text{-}N_1)$ remaining non-emitting junctions. N_1 is not known *a priori*; however, the evolution of the emission power in the 'normal', back-bending and forward-bending regions (see Fig. 5) suggests that a sizable fraction of the junctions does not emit. The reduction in emission frequency by a factor of *k* implies $V_{jct,1} = k_1 V_{jct,0}$, *i.e.*, $r_{jct,1} = k_1 \frac{I_0}{I_1} r_{jct,0}$. For the 1.037 V –data in Fig. 2 this yields a reduction of the junction resistance of the emitting junctions in the

back-bending regime by a factor of four. Considering the temperature dependence of R_c displayed in Fig. 1 this reduction would imply an increase in average temperature from 15 K to ~80 K, that is, above T_c. A similar analysis for the emission in the forward-bending regime yields k_2 = 0.81 and a reduction of the resistance of the emitting junctions by 1/12, corresponding to an average junction temperature of ~155 K, consistent with the notion that in the back-bending and forward bending regions the lateral temperature distribution is very inhomogeneous, consisting of hot spots with temperature above T_c and cold regions (near the ends of the stack) that are still superconducting, see Fig. 2b in ref. [18]. The large length/width aspect ratio of the mesa studied here – namely 12 – promotes this appearance of a largely normal conducting core of the mesa with the ends of the mesa still being superconducting. Since the *ab*-planes are equipotentials, the junction resistance, junction voltage and emission frequency are determined by the normal conducting short in the hot spot. Furthermore, with $V_0 = V_{1,2}$, it follows that $\frac{\bar{r}}{r_{jct,1,2}} = \frac{1/k - n_{1,2}}{1 - n_{1,2}} \geq 1$, with $n_{1,2} = N_{1,2}/N$. The average resistance of the unsynchronized junctions is larger than that of the synchronized junctions implying that the average temperature of the synchronized junctions is higher than the average of the remainder of the stack. Since cooling occurs predominantly through the base crystal, our results suggest that the emission originates from junctions located near the ends of the mesa and near its top (see Fig. 3b). A location near the top electrode would be consistent with the mode profile of the resonant cavity mode,

which has a maximum at the top electrode and a node near the interface with the base crystal [10].

As the mesa enters the forward-bending region the emission frequency displays an unusual re-entrant behavior as function of mesa voltage. We note though that as a function of increasing bias current the emission frequency monotonically decreases (see inset of Fig. 3). We attribute these features to the interplay of two opposite trends: (a) with increasing bias current self-heating increases, and, as ρ_c is a monotonically decreasing function of temperature, the junction resistance $r_{jct}[T(I)]$ decreases; (b) the quasi-particle voltage $r_{jct}[T(I)]I$ may increase or decrease depending on the magnitude of $\partial\rho_c/\partial T$. Since the IV-curve in the region of emission is almost vertical, this interplay will depend sensitively on the details of the temperature distribution in the mesa. Furthermore, cooling through the gold contact, even though generally considered much weaker than cooling through the base crystal [18], may affect the temperature balance as well. We expect though that as the mesa has fully made the transition into the forward–bending region, the emission frequency would increase again with mesa voltage.

The voltage dependence of the wavenumber at 10 K and 15 K displays a step near 16.5 cm^{-1}. The origin of these steps has not been established yet; however, as shown in Fig. 4, the emission line shape changes systematically when going across the step, the location of which is indicated by the vertical arrow. At lower wavenumbers – i.e., higher bias current – the lines develop shoulders at low intensities. This may indicate the excitation of additional modes, which could arise for example when the hot core completely separates the two ends. There are though no discernable

features in the IV-curve at the bias current of 18 mA corresponding to the step such as jumps that might indicate the motion of a hot spot, for instance [5, 9].

In summary, we have shown that Bi-2212 mesas can emit in two or even three distinct current regimes at certain mesa voltages, given the correct device dimensions and doping state of the material. This allows the properties of 'low-bias' and 'high-bias' THz emission regimes to be directly compared for the same mesa device. We find that while the emission frequency of the lowest current branch obeys the expected Josephson relation for a stack containing N IJJs, the observed THz frequency becomes significantly lower than this in the high current regime(s). While this behavior may at first seem counterintuitive, it is consistent with the stack becoming thermally inhomogeneous due to high DC power dissipation. As a hot spot shorts the junctions most effectively at the top of the stack, a subset of phase-locked junctions forms there, having $V_{jct} < V_{mesa}/N$ and thus a lower-than-expected Josephson frequency. This phenomenon must be taken into consideration when designing Bi-2212 mesa devices for emission in the high-bias regime.

Work at Argonne National Laboratory was funded by the Department of Energy, Office of Basic Energy Sciences, under Contract No. DE-AC02-06CH11357, which also funds Argonne's Center for Nanoscale Materials (CNM) where the patterning of the BSCCO mesas was performed. We thank R. Divan and L. Ocola for their help with sample fabrication.

Appendix

As indicated by the temperature dependence of R_c below T_c as shown in Fig. 1 there are non-superconducting junctions which contribute a temperature dependent contact resistance that must be properly evaluated in order to reliably estimate the superconducting junction voltages. Fig. 6 shows the low-bias part of the IV-curves revealing that prior to the first superconducting switching a non-linear voltage signal arises due to these non-superconducting junctions which can be well described by $I = aV + bV^3$ [22]. With increasing temperature the IV-curves approach a linear characteristics; at 60 K a contact resistance of 3.3 Ω is obtained which is the value of R_c just below T_c. At low temperatures the low-bias limit of the non-linear IV-curves reproduces the R_c-values shown in Fig. 1. For the sake of a uniform presentation, in the inset of Fig. 1 the voltage values have been corrected for a contact resistance of 3.3 Ω. Since self-heating in the 'normal' region is negligible, we use the non-linear IV-curves prior to switching in the evaluation of the Josephson relation shown in Fig. 3a. In the back-bending and forward-bending regions self-heating is predominant; therefore, as suggested by Fig. 6 a contact resistance of 3.3 Ω is appropriate. The high-bias data in Fig. 3a were obtained in this way. As shown by the dashed and solid lines in Fig. 6, there is some ambiguity in assigning the voltage values. However, this does not alter the conclusion of this work, namely that due to non-uniform temperature distributions along the *c*-axis the *ac*-Josephson relation in terms of the applied mesa voltage does not hold. This can be seen from Fig. 7, which shows for a temperature of 15 K the frequency versus voltage data as

measured, with a uniform contact resistance of 3.3 Ω and a contact resistance given by the non-linear IV prior to switching.

References

[1] L. Ozyuzer, A. E. Koshelev, C. Kurter, N. Gopalsami, Q. Li, M. Tachiki, K. Kadowaki, T. Yamamoto, H. Minami, H. Yamaguchi, T. Tachiki, K. E. Gray, W.-K. Kwok, U. Welp, Science **318**, 1291 (2007).

[2] R. Kleiner, F. Steinmeyer, G. Kunkel, P. Mueller, Phys. Rev. Lett. **68**, 2394 (1992).

[3] H. Minami, I. Kakeya, H. Yamaguchi, T. Yamamoto, K. Kadowaki, Appl. Phys. Lett. **95**, 232511 (2009).

[4] K. E. Gray, A. E. Koshelev, C. Kurter, K. Kadowaki, T. Yamamoto, H. Minami, H. Yamaguchi, M. Tachiki, W.-K. Kwok, U. Welp, IEEE Transactions on Applied Superconductivity **19**, 886 (2009).

[5] H. B. Wang, S. Guenon, J. Yuan, A. Iishi, S. Arisawa, T. Hatano, T. Yamashita, D. Koelle, R. Kleiner, Phys. Rev. Lett. **102**, 017006 (2009).

[6] M. Tsujimoto, K. Yamaki, K. Deguchi, T. Yamamoto, T. Kashiwagi, H. Minami, M. Tachiki, K. Kadowaki, R. A. Klemm, Phys. Rev. Lett. **105**, 037005 (2010).

[7] S. Guenon, M. Gruenzweig, B. Gross, J. Yuan, Z. G. Jiang, Y. Y. Zhong, M. Y. Li, A. Iishi, P. H. Wu, T. Hatano, R. G. Mints, E. Goldobin, D. Koelle, H. B. Wang, R. Kleiner, Phys. Rev. B **82**, 214506 (2010).

[8] K. Kadowaki, M. Tsujimoto , K. Yamaki, T. Yamamoto, T. Kashiwagi, H. Minami, M. Tachiki, R. A. Klemm, J. Phys. Soc. Jpn. **79**, 023703 (2010).

[9] H. B. Wang, S. Guenon, B. Gross, J. Yuan, Z. G. Jiang, Y. Y. Zhong, M. Gruenzweig, A. Iishi, P. H. Wu, T. Hatano, D. Koelle, R. Kleiner, Phys. Rev. Lett. **105**, 057002 (2010).

K. Yamaki, M. Tsujimoto, T. Yamamoto, A. Furukawa, T. Kashiwagi, H. Minami, K. Kadowaki, Opt. Express **19**, 3193 (2011).

[10] T. M. Benseman, A. E. Koshelev, K. E. Gray, W. K. Kwok, U. Welp, K. Kadowaki, M. Tachiki, T. Yamamoto, Phys. Rev. B **84**, 064523 (2011).

[11] T. Kashiwagi, M. Tsujimoto, T. Yamamoto, H. Minami, K. Yamaki, K. Delfanzari, K. Deguchi, N. Orita, T. Koike, R. Nakayama, T. Kitamura, M. Sawamura, S. Hagino, K. Ishida, K. Ivancovic, H. Asai, M. Tachiki, R. A. Klemm, K. Kadowaki, Jpn. J. Appl. Phys. **51**, 010113 (2012).

[12] M. Li, J. Yuan, N. Kinev, J. Li, B. Gross, S. Guenon, A. Ishii, K. Hirata, T. Hatano, D. Koelle, R. Kleiner, V. P. Koshelets, H. B. Wang, P. H. Wu, Phys. Rev. B **86**, 060505 (2012).

[13] M. Tsujimoto, T. Yamamoto, K. Delfanazari, R. Nakayama, T. Kitamura, M. Sawamura, T. Kashiwagi, H. Minami, K. Kadowaki, R. A. Klemm, Phys. Rev. Lett. **108**, 107006 (2012).

[14] T. M. Benseman, A. E. Koshelev, W.-K. Kwok, U. Welp, V. K. Vlasko-Vlasov, K. Kadowaki, H. Minami, C. Watanabe, J. Appl. Phys. **113**, 133902 (2013).

[15] A. E. Koshelev, Phys. Rev. B **78**, 174509 (2008).

[16] C. Kurter et al., IEEE Appl. Superconductivity **19**, 428 (2009); C. Kurter et al., Phys. Rev. B **81**, 224518 (2010); M. Suzuki, et al., Phys. Rev. Lett. **82**, 5361 (1999); H. B. Wang et al., Appl. Phys. Lett. **86**, 023504 (2005); J. C. Fenton, C. E. Gough, J. Appl. Phys. **94**, 4665 (2003); V. N. Zavaritsky, Phys. Rev. Lett. **92**, 259701 (2004); V. M. Krasnov, M. Sandberg, I. Zogaj, Phys. Rev. Lett., **94**, 077003 (2005).

[17] H. Minami, C. Watanabe, K. Sato, S. Sekimoto, T. Yamamoto, T. Kashiwaki, R. A. Klemm, K. Kadowaki, to be published.

[18] A. Yurgens, Phys. Rev. B **83**, 184501 (2011).

[19] B. Gross, S. Guenon, J. Yuan, M. Y. Li, J. Li, A. Ishii, R. G. Mints, T. Hatano, P. H. Wu, D. Koelle, H. B. Wang, R. Kleiner, Phys. Rev. B **86**, 094524 (2012).

[20] T. M. Benseman, PhD thesis, University of Cambridge 2007.

[21] T. M. Benseman, J. R. Cooper, C. L. Zentile, L. Lemberger, G. Balakrishnan, Phys. Rev. B **84**, 144503 (2011).

[22] J. Takeya, S. Akita, J. Shimoyama, K. Kishio, Physica C **261**, 21 (1996); A. Yurgens, D. Winkler, N. V. Zavaritsky, T. Claeson, Phys. Rev. Lett. **79**, 5122 (1997); Yu. I. Latyshev, T. Yamashita, L. N. Bulaevskii, M. J. Graf, A. V. Balatsky, M. P. Maley, Phys. Rev. Lett. **82**, 5345 (1999).

[23] Y. Omukai, I. Kakeya, M. Suzuki, Journal of Physics: Conference Series **400**, 052027 (2012).

Figure captions

Fig. 1. Temperature dependence of the c-axis resistivity measured directly at a low current of 10 μA (red symbols) and estimated from the sub-gap voltage as indicated by the solid line in the inset (orange squares). The inset shows the return branches of IV-curves measured at temperatures between 10 K and 100 K every 5 K. The dashed line indicates a resistance of 83 Ω, the resistance at T_c. The cross marks the bias point at 36.55 mA and 15 K at which a clear emission line is seen (see Fig. 2), even though the average mesa temperature is substantially above T_c.

Fig. 2. FTIR emission spectra at 15 K taken at mesa voltages of 1.018 V (closed circles) and 1.037 V (open squares) in the 'normal' (blue), back-bending (green) and forward-bending (red) regions. The bias current corresponding to each emission line is indicated.

Fig. 3. (a) Summary of the voltage dependence of the emission frequencies. The vertical dotted lines indicate the location of the spectra shown in Fig. 2. The solid line represents the Josephson relation. The inset shows the dependence of the emission frequency on bias current at 15 K.

(b) Schematic showing the temperature distribution and synchronized junctions (cross hatched) in a mesa. The curved vertical lines indicate the $T = T_c$ boundaries. In the back-bending region, the N_1 synchronized junctions have constant junction voltage whereas for the un-synchronized junctions the junction voltage increases

such that the total mesa voltage is the same as in the 'normal' region (blue dashed line).

Fig. 4. Evolution of the emission lines at 15 K in the vicinity of the step in wavenumber as seen in Fig. 3. The vertical arrow marks the location of the step. The inset shows a close-up of the IV-curve around the bias point of 18 mA corresponding to the step.

Fig. 5. Voltage dependence at 10 K (a) and 15 K (b) of the emission intensity in the 'normal', back-bending and forward-bending regions.

Fig. 6. Low-bias section of the IV-curves. Prior to the first superconducting switching a voltage signal appears that is well described as $I = aV+bV^3$ (dashed line) and which we attribute to non-superconducting junctions. At 60 K the IV-curve is linear, corresponding to a resistance of 3.3 Ω (solid line).

Fig. 7. Comparison of the effect of different treatments of the contact resistance on the frequency versus voltage diagram at 15 K.

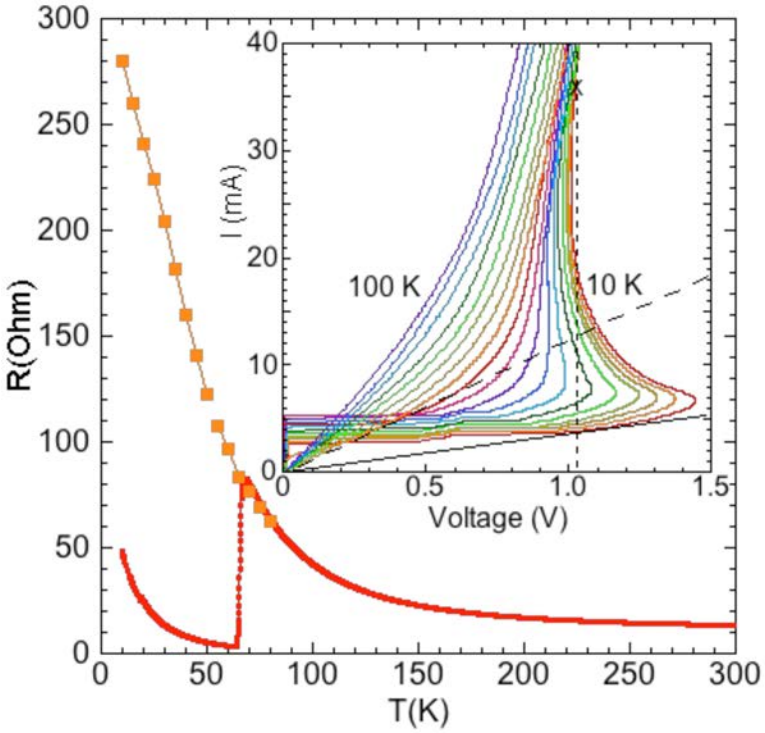

Fig. 1

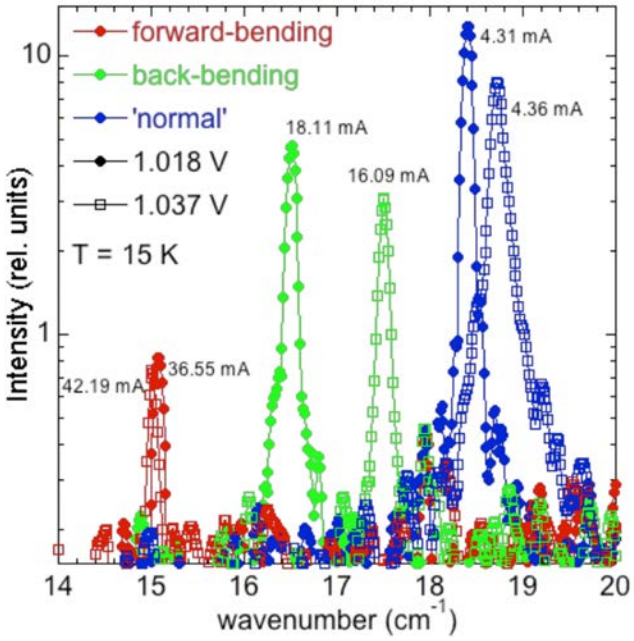
forward-bending
back-bending
'normal'
1.018 V
1.037 V
T = 15 K
Intensity (rel. units)
10
1
14
15
16
17
18
19
20
wavenumber (cm-1)
42.19 mA
36.55 mA
18.11 mA
16.09 mA
4.31 mA
4.36 mA

Fig. 2

a)

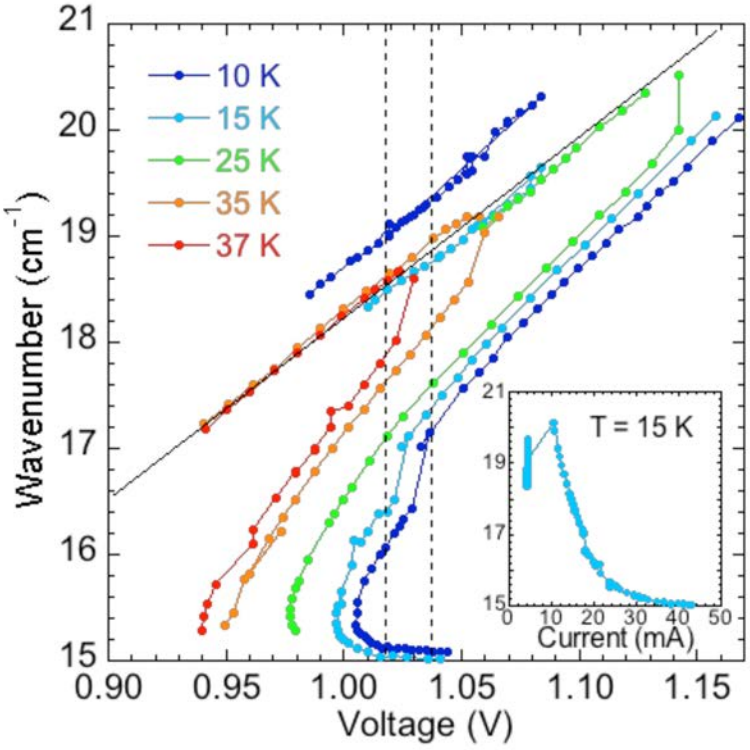
10 K
15 K
25 K
35 K
37 K
Wavenumber (cm^{-1})
Voltage (V)
T = 15 K
Current (mA)

b)

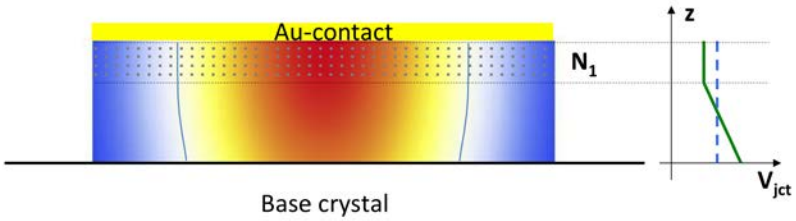
Au-contact
N_1
z
V_{jct}
Base crystal

Fig. 3

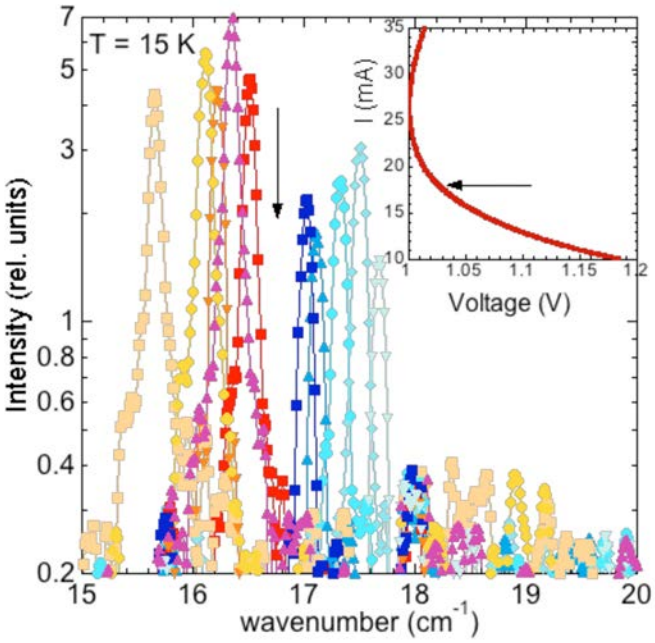

Fig. 4

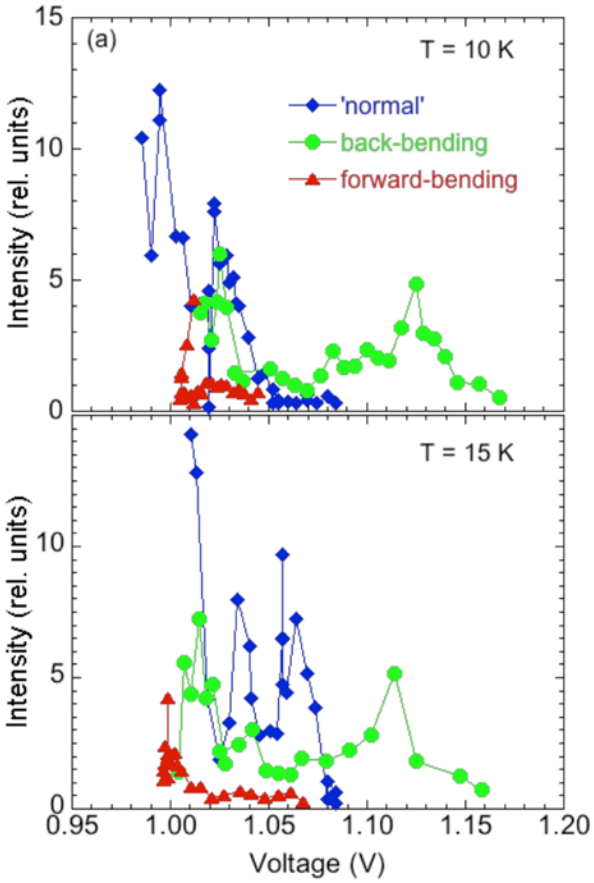
(a)
T = 10 K
'normal'
back-bending
forward-bending
Intensity (rel. units)
T = 15 K
Intensity (rel. units)
Voltage (V)
0
5
10
15
0.95
1.00
1.05
1.10
1.15
1.20

Fig. 5

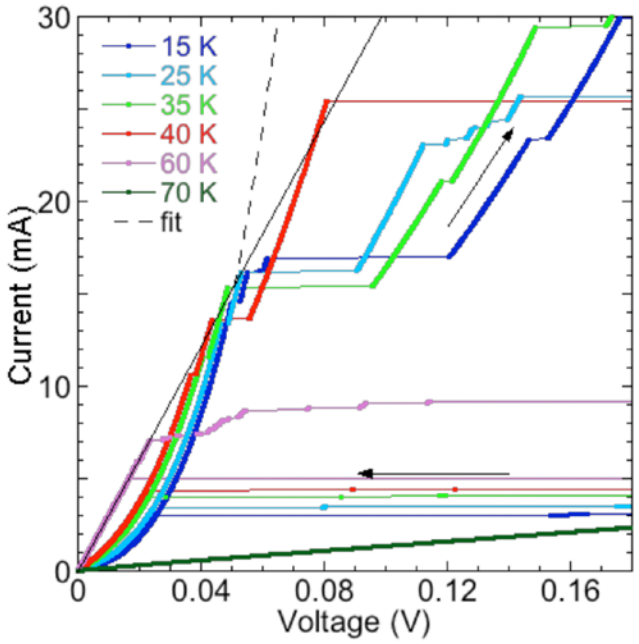
15 K
25 K
35 K
40 K
60 K
70 K
fit
Current (mA)
Voltage (V)
0
10
20
30
0
0.04
0.08
0.12
0.16

Fig. 6

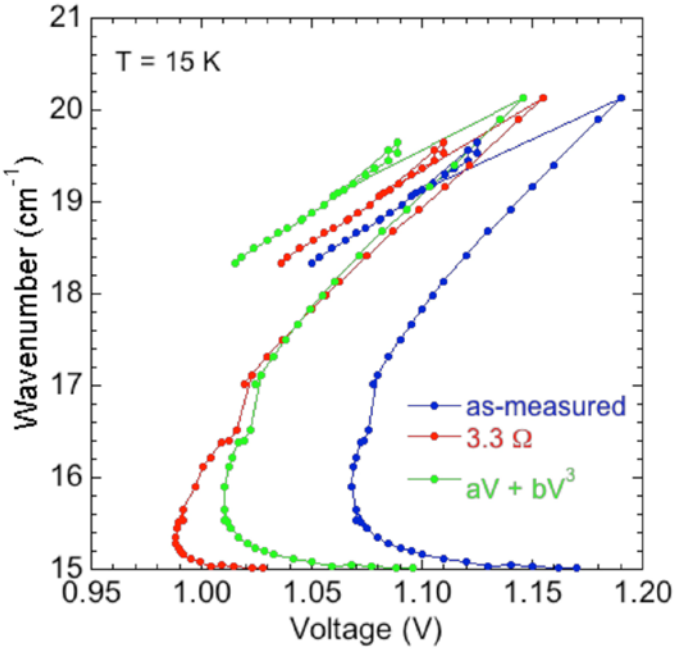
T = 15 K
Wavenumber (cm^{-1})
Voltage (V)
as-measured
3.3 Ω
aV + bV^3
21
20
19
18
17
16
15
0.95
1.00
1.05
1.10
1.15
1.20

Fig. 7